DR AMARNATH NATARAJAN (Orcid ID : 0000-0001-5067-0203)

Article type : Research Article

Symbiotic Prodrugs (SymProDs) Dual Targeting of NFkappaB and CDK

Sandeep Rana[1], Smit Kour[1], Yogesh A. Sonawane[1], Caroline M. Robb[1], Jacob I. Contreras[1], Smitha Kizhake[1], Muhammad Zahid[2], Adam R. Karpf[1,5] and Amarnath Natarajan*[,1,3,4,5]

[1]Eppley Institute for Research in Cancer and Allied Diseases,

[2]Department of Environmental, Agricultural and Occupational Health,

[3]Department of pharmaceutical Sciences,

[4]Department of Genetics Cell Biology and Anatomy,

[5]Fred and Pamela Buffett Cancer Center

University of Nebraska Medical Center, Omaha, Nebraska 68198, USA

Running title:

SymProDs: A novel class of therapeutics

Keywords:

NFkappaB, CDK, Prodrugs

***Address for Correspondence:**

Amarnath Natarajan PhD

Eppley Institute for Cancer Research and Allied Diseases

University of Nebraska Medical Center

986805 Nebraska Medical Center, Omaha, NE 68198-6805, USA
TEL: (402) 559-3793
FAX: (402) 559 8270
Email: anatarajan@unmc.edu

Disclosure of Conflicts of Interest: Authors have no conflict of interest to disclose

Abstract

The release of an active drug from the prodrug generates a pro-fragment that typically has no biological activity and could result in adverse effects. By combining two drugs wherein each drug acts as a pro-fragment of the other drug will eliminate the pro-fragment in the prodrug. Since they are prodrugs of each other and are symbiotic we termed these as symbiotic prodrugs (SymProDs). To test this idea, we generated SymProDs using NFκB inhibitors that contain the reactive α-methylene-γ-butyrolactone moiety and CDK inhibitors with solvent exposed secondary nitrogen atoms. We show that secondary amine prodrugs of α-methylene-γ-butyrolactone containing NFκB inhibitors undergo slow release over a 72h period. Using an alkyne tagged secondary amine prodrug of α-methylene-γ-butyrolactone containing NFκB inhibitor, we demonstrate target engagement. The NFκB-CDK SymProDs were ~20-200 fold less active against the corresponding CDK inhibitors in *in vitro* CDK kinase assays. Growth inhibition studies in a panel of ovarian cancer cell lines revealed potency trends of the SymProDs mirrored those of the single treatments suggesting their dissociation in cells. In conclusion our results suggest that SymProDs offer a productive path forward for advancing compounds with reactive functionality and can be used as dual targeting agents.

Introduction

An emerging concept is to incorporate prodrug design strategies early in the discovery phase as opposed to a salvage effort when delivery strategies fail (Rautio, Meanwell, Di, & Hageman, 2018). By definition a prodrug inherently has far less to no pharmacological activity when compared to the active drug but possess structural motifs that are liable to bioconversion that reveals the active drug (Albert, 1958). The release of the active drug from the prodrug also generates a pro-fragment that typically has no biological activity and, in some cases, could result in adverse effects. The antibacterial field was the first to design "mutual prodrugs" also known as "codrugs" wherein two drugs are conjugated through a labile linker (Baltzer et al., 1980). The marketed codrug sultamicillin, upon hydrolysis, releases ampicillin (β-lactamase antibiotic) and penicillanic acid sulfone (β-lactamase inhibitor). Bacteria develop resistance to β-lactamase antibiotics by elevating the expression of β-lactamase, which is targeted by penicillanic acid sulfone in sultamicillin thus restoring the efficacy of ampicillin.

Prodrug approaches to overcome high toxicity among chemotherapeutic agents have yielded promising results in preclinical and clinical settings. Widely used drugs such as doxorubicin are effective anticancer agents but suffer from offsite effects such as cardiomyopathy (Guthrie & Gibson, 1977). Aldoxorubicin (INNO-206) is a prodrug of doxorubicin that exploits the acidic tumor microenvironment to trigger the release of doxorubicin (Kratz et al., 2002). The cardiotoxicity profile of INNO-206 was far superior to doxorubicin in Phase II and III clinical trials (Cranmer, 2019). Platinum based drugs are another class that is widely used to treat an array of cancers also suffers from adverse effects. The reductive environment of the cancer cell allows the conversion of the kinetically inert Pt(IV) low spin d6 octahedral complex to the square planar Pt(II) derivatives by releasing the axial ligands (Hall, Mellor, Callaghan, & Hambley, 2007). The Gibson lab effectively exploited this by incorporating bioactive axial ligands to trigger the release of cisplatin along with COX and HDAC inhibitors in cancer cells (Babak et al., 2019; Harper et al., 2017; Petruzzella, Braude, Aldrich-Wright, Gandin, & Gibson, 2017; Petruzzella, Sirota, Solazzo, Gandin, & Gibson, 2018).

An array of targeted anticancer agents contains enone (α,β-unsaturated carbonyl) moieties that form covalent carbon-sulfur bonds with surface exposed sulfhydryl group of cysteine residues.

Examples include FDA approved irreversible inhibitors ibrutinib and afatinib that target burton tyrosine kinase and epidermal growth factor receptor, respectively (Pan et al., 2007; Solca et al., 2012). Chemoproteomic studies suggest that cysteinome is susceptible to covalent kinase inhibitors and since the off-targets also exhibit structure activity relationship a medicinal chemistry solution is viable to achieve kinase selectivity (Lanning et al., 2014). Another class of anticancer agents are pathway specific inhibitors that possess enone moieties which target the sulfhydryl groups of surface exposed cysteine residues. In particular sesquiterpene natural products that contain an α-methylene-γ-butyrolactone moiety that are known to form covalent adducts with proteins in the NFκB pathway. Parthenolide and isohelenin were early sesquiterpene lactones that were identified as NFκB pathway inhibitors (Bork, Schmitz, Kuhnt, Escher, & Heinrich, 1997). In an oral administered phase I trial, parthenolide was not detected in the plasma suggesting stability issues (Curry et al., 2004). Secondary amine-based prodrugs that masked the reactive enone of parthenolide improved stability while maintaining anticancer activity in tumor models (Hexum et al., 2015; Ren, Yu, & Kinghorn, 2016).

Using a cell-based TNFα-induced-IKKβ-mediated NFκB luciferase reporter screen, we identified an isatin-derived spirocyclic α-methylene-γ-butyrolactone (**19**) as an NFκB inhibitor that exhibited antitumor activity in an orthotopic model (Rana et al., 2016; Rana & Natarajan, 2013). Here for the first time we show target engagement in cells by a secondary amine prodrug of an NFκB inhibitor with the α-methylene-γ-butyrolactone moiety. Kinetic studies suggest slow release of the active enone. Several targeted agents contain secondary amines that are solvent exposed, for example CDK inhibitor AT7519 has a piperidine ring and CDK4/6 inhibitor palbociclib has a piperazine ring. Here we used the secondary amines of CDK inhibitors (AT7519 and palbociclib) to mask reactive α-methylene-γ-butyrolactone containing NFκB inhibitors (parthenolide and **19**) to generate 4 compounds (**5**-**8**) that were prodrugs of each other (symbiotic prodrugs - SymProDs). Evaluation of these SymProDs showed that the prodrug undergoes bioconversion to release the active enone in cancer cells.

Materials and Methods

All reagents were purchased from commercial sources and were used without further purification. Flash chromatography was carried out on silica gel (200–400 mesh). Thin layer chromatography (TLC) were run on pre-coated EMD silica gel 60 F254 plates and observed under UV light at 254 nm and with basic potassium permanganate dip. Column chromatography was performed with silica gel (230-400 mesh, grade 60, Fisher scientific, USA). ^{1}H NMR (400 – 600 MHz) and ^{13}C NMR (100 – 150 MHz) spectra were recorded in $CDCl_3$, DMSO-d_6 or CD_3OD on a Bruker instrument ($CDCl_3$ was 7.26 ppm for ^{1}H and 77.00 ppm for ^{13}C, DMSO-d_6 was 2.50 ppm for ^{1}H and 39.00 ppm for ^{13}C and CD_3OD was 3.31 ppm for ^{1}H and 49.3 for ^{13}C. Proton and carbon chemical shifts were reported in ppm relative to the signal from residual solvent proton and carbon. Preparative HPLC was carried out on 250 x 21.2 mm C-18 column using gradient conditions (10 – 100% B, flow rate = 6.0 mL/min, 39 min). The eluents used were: solvent A (H_2O with 0.1% Formic acid) and solvent B (CH_3CN with 0.1% Formic acid).

*4-((4-(trifluoromethyl)piperidin-1-yl)methyl)-3,4-dihydro-5H-spiro[furan-2,3'-indoline]-2',5-dione **(19-AP)***

4-(trifluoromethyl)piperidine (30 mg, 0.20 mmol) and TEA (50 µL) were added sequentially to a solution of 4-methylene-1'-(prop-2-yn-1-yl)-3,4-dihydro-5H-spiro[furan-2,3'-indoline]-2',5-dione (21 mg, 0.10 mmol) in ethanol (2 mL) at RT. The resulting solution was stirred for 3 h. Then the solvent was evaporated to afford the crude residue, which was purified by column chromatography to afford the desired compound as a mixture of diastereomers. ^{1}H NMR (DMSO-d_6) δ 10.75 (d, J = 9.0 Hz, 1H), 7.56 (dd, J = 7.5, 28.3 Hz, 1H), 7.34 (q, J = 7.7 Hz, 1H), 7.06 (dt, J = 7.6, 14.2 Hz, 1H), 6.90 (d, J = 7.8 Hz, 1H), 3.05 – 2.62 (m, 5H), 2.44 – 1.91 (m, 5H), 1.77 (d, J = 12.6 Hz, 2H), 1.43 (tdd, J = 4.7, 8.7, 10.7, 12.7 Hz, 2H). ^{13}C NMR (DMSO-d_6) δ 177.98, 176.28, 142.94, 131.56, 126.90, 125.48, 123.06, 110.88, 81.57, 58.14, 52.85, 51.23, 38.39, 38.17, 36.37, 35.09, 24.80, 24.70. $C_{18}H_{19}F_3N_2O_3$ $[M]^+$: 368.14; found 369.75.

*4-((dimethylamino)methyl)-3,4-dihydro-5H-spiro[furan-2,3'-indoline]-2',5-dione (**19-AP2**)*

To a solution of 4-methylene-1'-(prop-2-yn-1-yl)-3,4-dihydro-5H-spiro[furan-2,3'-indoline]-2',5-dione (60 mg, 0.28 mmol) in ethanol (3 mL) were added dimethylamine hydrochloride (45 mg, 0.56 mmol) and TEA (98 µL). The resulting solution was stirred for 4 h and progress of the reaction

was monitored by TLC. The solvent was evaporated to afford the crude residue, which was purified by column chromatography to afford the desired compound as a mixture of diastereomers. ^{1}H NMR (CD_3OD) δ 7.51 (d, J = 7.6 Hz, 1 Hz, 1H), 7.38 (t, J = 7.6 Hz, 1H), 7.13 (t, J = 7.6 Hz, 1H), 6.95 (d, J = 7.6 Hz, 1H), 3.89 – 3.61 (m, 2H), 3.40 – 3.34 (m, 1H), 3.24 – 3.18 (m, 1H), 2.93 (s, 6H), 2.55 – 2.49 (m, 1H). ^{13}C NMR (DMSO-d_6) δ 177.88, 176.29, 142.36, 131.54, 126.91, 125.55, 123.05, 110.86, 81.58, 59.84, 45.59, 38.60, 36.36, C14H16N2O3 $[M]^+$: 260.12; found 260.99.

*1-(prop-2-yn-1-yl)indoline-2,3-dione (**2**)*

To a solution of isatin (200 mg, 1.36 mmol) in anhydrous DMF (6 mL) cooled to 0°C under argon atmosphere was added 60% NaH (82 mg, 2.04 mmol). After 10 min, propargyl bromide (0.19 mL, 2.04 mmol, 80%) was added at −0°C, and the solution was allowed to warm to ambient temperature and stirred for 16h. Reaction mixture was washed with NH_4Cl and extracted with EtOAc. The organic phase was washed with brine, separated, dried over $MgSO_4$, and the solvent was evaporated in vacuo. The crude residue was purified by silica gel chromatography to afford the pure product (192 mg, 75%). ^{1}H NMR($CDCl_3$) δ 7.66 – 7.63 (m, 2H), 7.19 – 7.12 (m, 2H), 4.53 (d, J = 2.0 Hz, 2H), 2.30 (s, 1H). ^{13}C NMR ($CDCl_3$) δ 182.49, 157.13, 149.59, 138.39, 125.44, 124.18, 117.68, 111.06, 75.65, 73.31, 29.43. $C_{11}H_7NO_2$ $[M]^+$: 185.05; found 186.27.

Methyl 2-((3-hydroxy-2-oxo-1-(prop-2-yn-1-yl)indolin-3-yl)methyl)acrylate

In a round bottom flask, 1-(prop-2-yn-1-yl)indoline-2,3-dione (40 mg, 0.22 mmol) was dissolved in THF: water (2 ml, 2:1) followed by addition of Indium powder (49 mg, 0.43 mmol) and methyl 2-(bromomethyl) acrylate (77 mg, 0.43 mmol). Reaction was stirred at room temperature for 24h. Crude was dissolved in ethyl acetate and wash 1N HCl, and brine.

Crude mixture was column chromatographed using hexane and ethyl acetate gradient to obtain methyl 2-((3-hydroxy-2-oxo-1-(prop-2-yn-1-yl)indolin-3-yl)methyl)acrylate (33 mg, 54% yield). ^{1}H NMR ($CDCl_3$) δ 7.34 – 7.32 (m, 2H), 7.08 (t, J = 7.5 Hz, 1H), 7.03 (d, J = 8.0 Hz, 1H), 6.27 (s, 1H), 5.57 (s, 1H), 4.55 (dd, J = 2.5 Hz, 7.5 Hz, 1H), 4.35 (dd, J = 2.5 Hz, 7.5 Hz, 1H), 3.98 (br, 1H), 3.70 (s, 1H), 3.16 – 3.13 (m ,1 H), 2.76 – 2.73 (m, 1H), 2.24 – 2.23 (m, 1H). ^{13}C NMR ($CDCl_3$) δ 176.46, 168.23, 141.16, 134.06, 130.18, 129.67, 129.25, 124.60, 123.02, 109.42, 75.77, 72.48, 52.28, 40.23, 29.30. $C_{16}H_{15}NO_4$ $[M]^+$: 285.10; found 286.07.

*4-methylene-1'-(prop-2-yn-1-yl)-3,4-dihydro-5H-spiro[furan-2,3'-indoline]-2',5-dione (**3**)*

Taken methyl 2-((3-hydroxy-2-oxo-1-(prop-2-yn-1-yl)indolin-3-yl)methyl)acrylate (33 mg, 0.12 mmol) in 3 mL of DCM and cooled to 0º C followed by addition of *p*-toluene sulfonic acid (45 mg, 0.24 mmol) Crude mixture was diluted in ethyl acetate and washed with brines, dried $MgSO_4$, and column chromatographed to yield 4-methylene-1'-(prop-2-yn-1-yl)-3,4-dihydro-5H-spiro[furan-2,3'-indoline]-2',5-dione (18 mg, 61% yield). ^{1}H NMR ($CDCl_3$) δ 7.32 (dt, J = 7.5 Hz, 1 Hz, 1H), 7.34 (d, J = 7.0 Hz, 1H), 7.16 (dt, J = 7.5 Hz, 0.5 Hz, 1H), 7.11 (d, J = 8.0 Hz, 1H), 6.42 (t, J = 2.5 Hz, 1H), 5.81 (t, J = 2.5 Hz, 1H), 4.59 – 4.38 (m, 2H), 4.35 (dd, J = 2.5 Hz, 7.5 Hz, 1H), 3.45 – 3.10 (m, 2H), 2.28 (t, J = 2.5 Hz, 1H). ^{13}C NMR ($CDCl_3$) δ 172.57, 168.77, 141.99, 132.52, 131.26, 126.53, 124.24, 124.03, 123.33, 110.04, 79.24, 75.99, 73.09, 36.32, 29.64.

*1'-(prop-2-yn-1-yl)-4-((4-(trifluoromethyl)piperidin-1-yl)methyl)-3,4-dihydro-5H-spiro[furan-2,3'-indoline]-2',5-dione (**4**)*

4-(trifluoromethyl)piperidine (9 mL, 0.058 mmol) and TEA (20 mL) were added sequentially to a solution of 4-methylene-1'-(prop-2-yn-1-yl)-3,4-dihydro-5H-spiro[furan-2,3'-indoline]-2',5-dione (11 mg, 0.038 mmol) in methanol (1 mL) at RT. The resulting solution was stirred for 4 h. Then the solvent was evaporated to afford the crude residue, which was purified by column chromatography to afford the desired compound as a mixture of diastereomers. ^{1}H NMR (CD_3OD) δ 7.58 (d, J = 7.6 Hz, 1H), 7.53 – 7.49 (m, 1H), 7.26 – 7.21 (m, 2H), 4.57 – 4.55 (m, 2H), 3.98 – 3.75 (m, 3H), 3.50 – 3.45 (m, 1H), 3.17 – 3.13 (m, 2H), 2.96 – 2.91 (m, 1H), 2.78 (t, J = 2.4 Hz, 1H), 2.69 – 2.56 (m, 3H), 2.23 – 2.20 (m, 2H), 1.94 – 1.88 (m, 2H). UPLC−MS calculated for $C_{21}H_{21}F_3N_2O_3$ $[M]^+$: 406.41; found 406.79.

*4-((4-(6-((6-Acetyl-8-cyclopentyl-5-methyl-7-oxo-7,8-dihydropyrido[2,3-d]pyrimidin-2-yl)amino)pyridin-3-yl)piperazin-1-yl)methyl)-3,4-dihydro-5H-spiro[furan-2,3'-indoline]-2',5-dione (**5**)*

To a solution of 4-methylene-3,4-dihydro-5*H*-spiro[furan-2,3'-indoline]-2',5-dione (20 mg, 0.093 mmol), triethylamine in methanol (2 mL) was added palbociclib (42 mg, 0.093 mmol) and the mixture was stirred for 48 h. Then the mixture was concentrated in vacuo and purified by prep HPLC (Yield 10 mg, 16%). ^{1}H NMR (DMSO-d_6) δ 10.24 (s, 1H), 10.08 (d, *J* = 3.5 Hz, 1H), 8.95 (s, 1H), 8.04 (dd, *J* = 3.1, 12.2 Hz, 1H), 7.84 (dd, *J* = 2.6, 9.0 Hz, 1H), 7.66 – 7.40 (m, 1H), 7.27 – 7.02 (m, 2H), 7.02 – 6.87 (m, 1H), 6.77 (dd, *J* = 7.7, 1H), 6.02 (d, *J* = 11.6 Hz, 1H), 5.95 (d, *J* = 1.6 Hz, 1H), 5.82 (d, *J* =

8.8 Hz, 1H), 5.46 (d, *J* = 1.5 Hz, 1H), 3.52 (s, 1H), 3.44 (s, 1H), 3.16 (d, *J* = 5.3 Hz, 2H), 3.08 (s, 1H), 2.94 (d, 1H), 2.89 – 2.52 (m, 3H), 2.44 (t, *J* = 5.6 Hz, 1H), 2.42 (s, 2H), 2.43 – 2.10 (m, 5H), 1.99 – 1.85 (m, 2H), 1.80 – 1.71 (m, 1H), 1.62 – 1.53 (m, 1H), 0.93 (t, *J* = 7.1 Hz, 3H). ^{13}C NMR (DMSO-d_6) δ 202.90, 178.87, 167.23, 155.21, 142.02, 135.11, 130.98, 129.47, 128.40, 125.20, 121.55, 109.92, 99.98, 76.00, 51.98, 40.60, 40.43, 40.27, 40.10, 39.93, 39.41, 38.81, 31.78, 28.02, 25.57, 14.09 UPLC−MS calculated for $C_{36}H_{38}N_8O_5$ $[M]^+$: 662.29; found 663.30.

*6-Acetyl-8-cyclopentyl-2-((5-(4-(((3R,3aS,9aR,10aS,10bS,E)-6,9a-dimethyl-2-oxo-2,3,3a,4,5,8,9,9a,10a,10b-decahydrooxireno[2',3':9,10]cyclodeca[1,2-b]furan-3-yl)methyl)piperazin-1-yl)pyridin-2-yl)amino)-5-methylpyrido[2,3-d]pyrimidin-7(8H)-one (**6**)*

To a solution of parthenolide (25 mg, 0.100 mmol), triethylamine in methanol (2 mL) was added palbociclib (45 mg, 0.100 mmol) and the mixture was stirred for 48 h. Then the mixture was concentrated in vacuo and purified by prep HPLC (Yield 16 mg, 23%). ^{1}H NMR (DMSO-d_6) δ 10.08 (d, 1H), 8.95 (s, 1H), 8.05 (dd, *J* = 3.0, 1H), 7.84 (t, *J* = 9.7 Hz, 1H), 7.51 – 7.41 (m, 1H), 5.86 – 5.78 (m, 1H), 3.98 (t, *J* = 9.1 Hz, 1H), 3.17 (d, *J* = 5.1 Hz, 4H), 3.06 (t, *J* = 4.8 Hz, 1H), 2.89 – 2.78 (m, 2H), 2.65 (dd, *J* = 7.6, 2H), 2.42 (s, 3H), 2.31 (s, 4H), 2.19 (d, 4H), 2.02 (t, 2H), 1.82 (d, 6H), 1.61 (d, 6H), 1.20 (s, 3H). ^{13}C NMR (DMSO-d_6) δ 175.82, 134.70, 125.12, 81.84, 68,28, 65.79, 61.59, 59.14, 48.24, 45.22, 40.99, 40,61, 40.27, 40.10, 39.93, 39.59, 36.50, 29.08, 24.18, 17.33, 17.01UPLC−MS calculated for $C_{39}H_{49}N_7O_5$ $[M]^+$: 695.38; found 696.38.

*4-(2,6-dichlorobenzamido)-N-(1-((2',5-dioxo-4,5-dihydro-3H-spiro[furan-2,3'-indolin]-4-yl)methyl)piperidin-4-yl)-1H-pyrazole-3-carboxamide (**7**)*

To a solution of 4-methylene-3,4-dihydro-5*H*-spiro[furan-2,3'-indoline]-2',5-dione (16 mg, 0.074 mmol), triethylamine in methanol (2 mL) was added AT7519 (31 mg, 0.074 mmol) and the mixture was stirred for 48 h. Then the mixture was concentrated in vacuo and purified by prep HPLC (Yield 8 mg, 18%). ^{1}H NMR (DMSO-d_6) δ 10.76 (d, 1H), 10.27 (d, 1H), 10.16 (d, *J* = 8.6 Hz, 1H), 8.43 – 8.22 (m, 2H), 7.70 – 7.42 (m, 3H), 7.28 – 6.87 (m, 3H), 6.86 – 6.69 (m, 1H), 3.58 – 3.43 (m, 2H), 3.24 (s, 2H), 2.94 – 2.61 (m, 2H), 2.43 – 2.05 (m, 2H), 2.04 – 1.83 (m, 2H), 1.80 – 1.37 (m, 4H). ^{13}C NMR (DMSO-d_6) δ 178.50, 173.77, 163.12, 159.87, 141.15, 134.86, 131.40, 130.85, 130.76, 130.62, 128.53, 127.94, 124.52, 123.97, 123.34, 122.14, 120.97, 120.93, 109.12, 74.04, 60.14, 51.82,

51.49, 50.64, 45.54, 37.91, 37.77, 30.53. LC−MS calculated for $C_{28}H_{26}Cl_2N_6O_5$ $[M]^+$: 596.13; found 597.2.

*4-(2,6-dichlorobenzamido)-N-(1-(((3R,3aS,9aR,10aS,10bS,E)-6,9a-dimethyl-2-oxo-2,3,3a,4,5,8,9,9a,10a,10b-decahydrooxireno[2',3':9,10]cyclodeca[1,2-b]furan-3-yl)methyl)piperidin-4-yl)-1H-pyrazole-3-carboxamide (**8**)*

To a solution of parthenolide (16 mg, 0.064 mmol), triethylamine (20 µL) in methanol (2 mL) was added AT7519 (30 mg, 0.070 mmol) and the mixture was stirred for 48 h. Then the mixture was concentrated in vacuo and purified by prep HPLC (Yield 10 mg, 25%). ^{1}H NMR (DMSO-d_6) δ 13.39 (s, 1H), 10.17 (s, 1H), 8.37 – 8.28 (m, 2H), 7.61 – 7.49 (m, 3H), 5.25 – 5.17 (m, 1H), 3.95 (t, J = 9.1 Hz, 1H), 3.72 (m, 1H), 2.84 (d, J = 11.5 Hz, 1H), 2.76 (d, J = 9.1 Hz, 2H), 2.70 – 2.53 (m, 3H), 2.54 (s, 2H), 2.35 (m, 1H), 2.26 – 2.06 (m, 2H), 2.06 – 1.92 (m, 3H), 1.66 – 1.54 (m,, 5H), 1.20 (s, 3H), 1.12 (td, J = 5.8, 12.7 Hz, 1H). ^{13}C NMR (DMSO-d_6) δ 177.33, 163.07, 160.72, 135.82, 135.08, 133.39, 132.34, 131.70, 128.88, 124.60, 121.92, 121.10, 82.05, 66.14, 61.55, 56.86, 53.88, 52.74, 47.99, 46.41, 45.62, 41.09, 36.62, 31.88, 31.59, 29.48, 24.08, 17.30, 17.2 LC-MS calculated for $C_{31}H_{37}Cl_2N_5O_5$ [M]+: 629.2; found 630.3.

Cell lines and Materials: The cell lines were assembled by Dr. Karpf and the original source is in parenthesis. Cell line identity was confirmed by STR testing and were confirmed to be mycoplasma free. Typical experiments were conducted with cells passaged at least 3-times following a thaw. A2780 (ATCC), OVSAHO (Japanese collection of research bioresources cell bank) and SNU119 (Korean cell line bank) cells were maintained in RPMI medium (HyClone #SH30027.01) and OVCAR4 (NCI division of cancer treatment and diagnosis cell line repository), OVCAR5 (Dr. Mitra, Indiana University), OVCAR8 (NCI division of cancer treatment and diagnosis cell line repository), Caov3 (Dr. Mitra, Indiana University), FT282-E1 (Dr. Drapkin – PMCID: PMC4517944) and FT282-C11 (Dr. Karpf, clonal isolate – PMCID: PMC6244393) cells were maintained in DMEM high glucose medium (HyClone #SH30022.01). All cell lines were supplemented with 10% FBS (Gibco #26140-079) and 1% Penicillin-Streptomycin (HyClone # SV30010), cultured at 5% CO_2, 37°C.

Immunoblotting: A2780 cells were treated with 20 µM of alkyne tagged 19-AP2 (analog 4) for 48h. Lysates were prepared with lysis buffer consisting of 50 mM Tris (pH 7.5), 100 mM NaCl, 2 mM EDTA, 1% NP-40, 0.1% SDS, 1mM PMSF, 1X protease and phosphatase inhibitors cocktails. Lysed

cell extracts were incubated for 30 min on ice and vortexed every 15 min. Lysates were centrifuged at 14,000 g for 10 min at 4°C. Finally, supernatant was collected, and protein was quantified using BCA protein assay kit (Pierce #23225). 2mg/mL (360 µL) of protein was subjected to click chemistry. Biotin-TAMRA-Azide (20 µL, 10 mM stock solution in DMSO); tris(2-carboxyethyl)phosphine hydrochloride (TCEP) (10 µL, 100 mM freshly prepared stock solution in water); tris[(1-benzyl-1-H-1,2,3-triazol-4-yl)methyl]amine (TBTA) (20 µL, 13.5 mM stock solution in 3:1 tertbutanol:DMSO); $CuSO_4 \cdot 5H_2O$ (10 µL, 100 mM freshly prepared stock solution in water) for a total reaction volume of 60 µL and added 580 µL of PBS buffer (1X) to make total volume of 1 mL. Samples were incubated for 3 hours at the room temperature and 15 µL of samples was stored at -20 °C as control. The samples were then separated on a monomeric avidin column according to the manufacturer's instructions (Pierce) at 4 °C. After the samples were collected, they were concentrated using a 10 kDa molecular weight cutoff filter (Amicon), ddH_2O (50 mL) was added, centrifuged, and finally the samples were freeze-dried. Protein samples were run on 4-15% gradient SDS-PAGE gels (BioRad) in 1x Tris- Glycine-SDS buffer at 120V for 60min. Proteins were transferred onto PVDF membranes by using semi-dry transfer method. Membranes were blocked with 5% fat-free milk in 1x Tris bufferd saline with 0.1% Tween (TBST) for 1h at RT. Membranes were incubated overnight at 4°C with primary antibodies against IKKβ (CST #8943), p65 (SantaCruz #sc372), IκBα (CST #4812), IKKγ (Millipore #05-631) and α-Tubulin (CST #3873) made in 5% fat-free milk in 1x TBST. Membranes were incubated with the appropriate HRP-conjugated secondary antibody (Thermo Fisher Scientific #G-21040 and #32460) for 1h at RT. All membranes washes were performed using 1x TBST buffer (20 mM Tris-HCl (pH 7.5), 150 mM NaCl, 0.1% Tween-20) 3 times for 10 min. ECL Prime (GE Healthcare #RPB2236) was used to develop blots.

Growth inhibition assay: Cells were seeded at density of 4000 cells/well in a 96 well plate in RPMI and allowed to adhere overnight at 5% CO_2, 37°C. On the following day, cells were treated with different concentrations of analog 19, analog 19-AP1 and analog 19-AP2. PrestoBlue reagent (Invitrogen) was added according to manufacturer's instruction to cells after 72 h drug treatment to assess the growth inhibition. Fluorescence excitation/ emission was measured at 560/590 nm using plate reader SpectraMax M5^e instrument. IC_{50} was determined using SigmaPlot (Systat Software, San Jose, CA).

Cysteine Reactivity Assay: 200mM tris base buffer was diluted in 1X methanol (pH ~ 8.8). L-cysteine reduced was diluted to a final concentration of 250 μM in assay buffer (100 mM Tris pH 8.8, 50% methanol as a co-solvent). In triplicate, 100 μL of L-cysteine (250 μM) in assay buffer was added to each well in a clear, flat-bottom 96-well plate (Costar, Corning). Analog **19** (2.5 μL, 10 mM stock, 250 μM final), analog **19-AP2** (2.5 μL, 10 mM stock, 250 μM final) and DMSO were added to each well in triplicate (10 min interval) and incubated at room temperature for 0-60 min. Upon incubation completion, Ellman's reagent (5 μL, 100 mM stock in DMSO, final concentration 5 mM) was added and the reaction incubated at room temperature for 10 minutes. Absorbance was measured at 412 nM on a plate reader (SpectramaxM5^{e}).

Glutathione Assay: Standard preparation – From the 1 mg GSH Standard (10 μg/ μL) provided, add H2O to make a working std (2.5 mg/mL). Make dilutions with sample buffer provided to give 11 standards of 100 μL each ranging from 0.5 mg/ml of GSH up to 0.0005 mg/mL of GSH. Standard 12 is blank. Standards were prepared in duplicates.

Cell lysate preparation – 1×10^6 Ovarian cancer cells (A2780 and OVSAHO) rinsed 3X with ice-cold 1X PBS, were harvested and centrifuged at 14,000 rpm for 15 minutes at 4°C to pellet the cells. 100 μL of the lysis buffer from the abcam kit (ab 65322) was added to the tubes and incubated on ice for 10 min. Centrifuge at 14,000 rpm for 10 minutes at 4°C to pellet the debris. 75 μL supernatant was carefully removed and transferred to an ice-cold tube. 25 μL 4M PCA was added to the supernatant to precipitate the proteins. The solution was vortexed and incubated on ice for 5 min, centrifuged at 14,000 rpm for 5 minutes at 4°C to pellet the precipitate. 88 μL supernatant was carefully transferred to another chilled tube. 30 μL ice cold 2 M KOH was added to this supernatant and mixed well to neutralize the PCA. pH was adjusted to 6.5 – 8 range with 0.01M KOH. Proteins were pelleted at 14,000 rpm for 15 minutes and 100 μL supernatant was transferred to another chilled tube.

Sample preparation – 40 μL of the lysate was diluted to 100 μL with buffer. 6 half dilutions were made for each cell lysate in duplicates.

Detection reagent – 1:1 volume of GST reagent and MCB (monochlorobimane) were mixed to create a master mix. 4 μL of this mix was added per well.

Detection – The assay was done in a 96 well black, clear bottom plate and the final reaction volume was 104 µL. The plate was incubated at 37°C and read on the Spectramax in the kinetic mode every 2 minutes for an hour. Flourescence was measured at Ex/Em 380/461.

Data processing – Data was analyzed and a time point was picked where the curves were flat indicating a stable GSH/GSSG-MCB adduct formation. The time point used was 28 minutes. Standard graphs were plotted for both high and low concentrations and only the low concentration demonstrated linearity. All values were blank subtracted to obtained corrected readings. Concentration of GSH (mg/mL) was calculated for the highest concentration in each cell line from the standard graph. Dilution factor (from PCA and KOH addition) was accounted for and the corrected blank subtracted values were obtained. The final values were expressed as GSH concentration in µM /10^6 cells.

^{19}F NMR Experiment: A solution of glutathione (55 mg) in water (3.58 mL) and DMSO (8.35 mL) was titrated to pH 7.4 using 1.0 M NaOH (water). Next, glutathione solution (2.7 mL, pH 7.4) was treated with a 300 µL (10 mM stock solution of compound **19-AP2** in DMSO). An aliquot (500µL of **19-AP2** and 50 µL DMSO-d_6) was transferred to NMR tube for ^{19}F NMR at 0, 24, 48 and 72h at 80 °C.

Results and Discussion

Reaction of 4-methylene-3,4-dihydro-5H-spiro(furan-2,3'-indoline)-2',5-dione (**19**)(Rana et al., 2016; Rana & Natarajan, 2013) with 4-trifluoropiperidine in ethanol resulted in the corresponding amino prodrugs 4-((4-(trifluoromethyl)piperidin-1-yl)methyl)-3,4-dihydro-5H-spiro(furan-2,3'-indoline)-2',5-dione (**19-AP**) as a mixture of diastereomers (Figure 1A). The α-methylene-γ-butyrolactone moiety on analog **19** is reactive toward biological nucleophiles such as glutathione and cysteine. To determine if secondary amine prodrug of **19** (**19-AP**) results in improved stability, we compared the reactivity of analog **19** and the prodrug **19-AP** in a cysteine binding assay using Ellman's reagent (Figure 1B).(Zaro, Whitby, Lum, & Cravatt, 2016) Analog **19** reacted rapidly with free cysteine whereas amine-prodrug **19-AP** is more stable under similar conditions. These studies show that the amine-based prodrugs of α-methylene-γ-butyrolactone containing compounds are stable to biological nucleophiles. Next, to assess the kinetics of the release of the active compound **19** from the prodrug **19-AP**, we monitored the release of 4-trifluoropiperidine from the prodrug **19-AP** using ^{19}F-NMR spectroscopy following the method reported by the Colby group.(Woods, Mo, Bieberich, Alavanja, & Colby, 2011) The ^{19}F NMR studies showed a time-dependent disappearance of the CF_3 signal on **19-AP** and corresponding appearance of the CF_3 signal on 4-trifluoromethylpiperidine (Figure 1C). This observation is consistent with previously reported studies with a prodrug of parthenolide. These studies clearly show that **19-AP** is more stable to biological nucleophiles and the prodrug is hydrolyzed slowly to release the active compound **19** over a 72h period.

We next explored whether prodrug **19-AP** covalently binds to NFκB pathway proteins in cells. Scheme 1 summarizes the synthesis of an alkyne-tagged prodrug (**4**) that is suitable for *in situ* click chemistry. Briefly, commercially available isatin (**1**) was stirred with propargyl bromide and potassium carbonate in DMF to yield substituted isatin (**2**). Intermediate **2** was subjected to Indium catalyzed Barbier-type reaction followed by a acid-catalyzed cyclization to yield compound **3**.(Rana & Natarajan, 2013) Treatment of **3** with 4-trifluoromethylpiperidine and triethylamine in methanol resulted in desired alkyne-tagged analog **4**.

To determine target engagement in cells, we subjected cancer cells (A2780) with the alkyne-tagged prodrug **4** for 48h. Cells were then harvested, washed and pelleted. Unbound **4** was removed by extensively washing the cell pellet. The cell pellets were lysed, and 2 mg/mL of lysates were

subjected to click chemistry with TAMRA-Biotin-Azide trifunctional probe (10 mM stock, 20 μL, click chemistry tools), and other click reagents (TCEP, 100 mM stock, 20 μL; TBTA 13.5 mM stock, 20 μL and $CuSO_4$ 100 mM stock, 10 μL) to make total volume of 1 mL. The reaction was incubated for 3h at RT. The lysates were incubated with monomeric avidin beads for additional 1h. The sample was washed with 15 mL elution buffer to remove unbound proteins followed by multiple washing with regeneration buffer (15 mL) to cleave biotin-monomeric avidin bond (Pierce® Monomeric Avidin Kit, ThermoScientific, Cat # 20227). The collected regeneration sample was washed with an excess of water (50 mL) to remove salts and freeze dried to yield tagged protein powder (Note: Even after multiple washing, proteins samples contained significant amounts of salts). Protein powder was dissolved in buffer and subjected to Western blot analyses. The membranes were probed for NFκB pathway proteins IKKβ, RELA, IκBα and IKKγ (Figure 2). We observed covalent binding of IKKβ, and RELA proteins to analog **4** but not IκBα or IKKγ proteins despite presence of surface exposed cysteine residues. This is the first report that shows that an amine-based prodrug of α-methylene-γ-butyrolactone containing NFκB inhibitor selectively engaged NFκB pathway proteins RELA and IKKβ in cells. This confirms the release of the parent eneone (**3**) from prodrug **4**, which irreversibly binds to RELA and IKKβ.

We next evaluated if the amine-prodrugs (**19-AP** and **19-AP2**) inhibited cancer cell growth. Analogs **19**, **19-AP** and **19-AP2** were screened in ovarian cancer lines (A2780, and OVSAHO) and immortalized fallopian tube epithelial cells (FT282E1) in a 72h growth inhibition assay (Figure 3). In A2780 and FT282E1 cell lines, amine-prodrugs are ~2 – 3 fold less active than the parent compound **19** whereas amine-prodrugs **19-AP** and **19-AP2** are more potent in the OVSAHO cell line (Figure 3). To determine if this difference in activities was due to quenching of the eneone by the thiol nucleophile glutathione (GSH) or release kinetics, we determined cellular GSH levels in the ovarian cancer cell lines (Supplementary Figure S1). We did not observe any correlation between the GSH levels and the activity (Figure 3D). The growth inhibitory activity observed with **19-AP** and **19-AP2** suggests that the active eneones are released because others and we have previously reported that reduction of the exocyclic double bond in compounds with α-methylene-γ-butyrolactone resulted in a complete loss of activity.(Guzman et al., 2007; Holcomb et al., 2012; Nasim & Crooks, 2008;

Neelakantan, Nasim, Guzman, Jordan, & Crooks, 2009; Pei et al., 2016; Rana et al., 2016; Shanmugam et al., 2011; Shanmugam et al., 2010)

Two plausible mechanisms for the conversion of amine-prodrugs to parent analogs have been previously suggested.(Holcomb et al., 2012; Shanmugam et al., 2011; Shanmugam et al., 2010) Figure 3E summarizes the plausible mechanisms for the conversion of **19-AP** to analog **19**. In the first case, GSH functions as a nucleophile to drive the E2 elimination of the protonated piperidine nitrogen of **19-AP** to generate **19** (Figure 3E, I-1). In the second case, the secondary amine in **19-AP** is oxidized facilitating a Cope like elimination to generate **19** (Figure 3E, I-2). Since it is known that the GSH levels are elevated in cancer cell lines (Balendiran, Dabur, & Fraser, 2004) the former mechanism is generally accepted for the release of the active drug. However, in our hands, we did not see a correlation between the GSH levels and growth inhibition (Figure 3D). This suggests that analog **19** is probably generated from **19-AP** through the later mechanism.

Our studies show that secondary amine-based prodrugs generated from **19** engages RELA and IKKβ in cells and inhibits cancer cell growth. Therefore, we hypothesized that prodrugs of **19** generated with secondary amine containing inhibitors that target a complimentary pathway will allow simultaneous targeting of two pathways. To test this hypothesis, we synthesized two prodrugs each of analog **19** (**5** and **7**) and parthenolide (**6** and **8**) with CDK4/6 inhibitor palbociclib (**5** and **6**), which has been approved for the treatment of metastatic breast cancer patients and AT7519 (**7** and **8**), which is a pan-CDK inhibitor currently in clinical trials (Figure 4A).

To evaluate the change *in vitro* efficacy of the palbociclib hybrids (**5** and **6**) for CDK4 and CDK6, we performed cell-free assays (Figure 4B). Although the CDK6:palbociclib co-crystal structure (pdb id: 5L21) suggests that the piperazine nitrogen atom is solvent exposed, palbociclib hybrids with **19** and parthenolide (hybrid **5** and **6**) were less active than palbociclib against CDK4 and CDK6. The **19**-palbociclib hybrid (**5**) was ~100- and ~20-fold less potent than palbociclib against CDK4 and CDK6 respectively. The parthenolide-palbociclib hybrid (**6**) was ~200- and ~50-fold less potent than palbociclib against CDK4 and CDK6 respectively. It is clear that CDK6 tolerates alkylation of piperazine nitrogen atom better than CDK4. We observed a similar effect during the development of a CDK6 selective degrader using PROTAC based strategy.(Rana et al., 2019) Moreover, the larger size of parthenolide compared to analog **19** is probably responsible for a greater

loss of activity of the parthenolide-hybrid (**6**) compared to analog **19**-hybrid (**5**). Nevertheless, it is clear that blocking the piperazine nitrogen on palbociclib results in significant loss of activity, which will be regained in the cells upon the release of the NFκB inhibitors (analog **19** and parthenolide). Therefore, we termed these hybrids as symbiotic prodrugs (SymProDs).

CDK4, CDK5, and CDK6 show a negative Pearson and Spearman correlation with RELA each with a p value < 0.05 (depmap.org) suggesting that simultaneous targeting of these CDKs and RELA would result in synergistic effects. To test this idea, we evaluated the (palbociclib, AT7519, **19**, parthenolide) four SymProDs (**5**-**8**) and their corresponding 1:1 mixture in growth inhibition assays in a panel of five cell lines (Figure 5). Among the inhibitors treated as single agents the potency irrespective of the cell line ranked as follows: AT7519 > **19** > parthenolide > palbociclib. The 1:1 combination treatment showed dose-response across all cell lines, and the potency mirrored the dominant single agent treatment. Surprisingly, SymProDs were less potent than the corresponding 1:1 combinational treatment. As expected, the AT7519 based SymProDs were more potent than the palbociclib based SymProDs. The potency trends of the hybrids followed those of the single treatments which suggests that the SymProDs are dissociating in the cells. The average combination index (^{Ave}CI) at effective dose (ED) 50, 75 and 90 for SymProD 5 in OVSAHO cells was 0.9 indicating weak synergism while the ^{Ave}CI > 1.0 for the FT282E1 cells.

Although significant advancements have been made to treat cancer, ovarian cancer remains the leading cause of gynecological cancer deaths in the United States. Several reports show that NFκB pathway is dysregulated in ovarian cancer. (House et al., 2017; Lee et al., 2007; Leizer et al., 2011; Sagher et al., 2014; White et al., 2011) In a panel of ovarian cancer cell lines, we observe elevated levels of RELA when compared to immortalized fallopian tube epithelial cell lines, which are an appropriate normal control for most ovarian cancers(Perets & Drapkin, 2016) (Supplementary Figure S2). Consistently, analyses of the TCGA data from 17 cancer types show that RELA (p65) expression is the highest in ovarian tumors (Supplementary Figure S3). These suggest that targeting the NFκB pathway proteins (RELA and IKKβ) is a viable therapeutic strategy for ovarian cancer. Moreover, CDK4/6 has been implicated in ovarian cancer tumorigenesis and resistance to therapy.(Dall'Acqua et al., 2017; Gao et al., 2017) Therefore, we wanted to compare the efficacy of the palbociclib based SymProDs (**5** and **6**) with the corresponding (1:1) mixtures in and expanded panel of 9 ovarian cancer

(CaOV3, OVCAR5, OVCAR8, A2780, Kuramochi, OVCAR4, OVSAHO, SKOV3 and SNU119) and 2 immortalized fallopian tube epithelial cell lines (FT282E1 and FT282C11) (Figure 6).

Analyses of the data show that on an average SymProD **6** was ~7-fold less potent than the corresponding 1:1 mixture, while the **19**-based SymProD **5** was equipotent to the corresponding 1:1 mixture. The ^{Ave}CI for SymProD 5 in SKOV3 cells was 0.2 indicating strong synergism. Although the parthenolide:palbociclib (1:1) mixture was on an average ~2-fold more potent than the **19**:palbociclib (1:1) mixture, the **19**-palbociclib SymProD **5** was ~3-fold more potent than the parthenolide-palbociclib SymProD **6**. This could be attributed to lower potency of parthenolide-palbociclib SymProD **6** in the *in vitro* kinase assays. An alternate possibility is that the release of palbociclib from **19** is more efficient than the release of palbociclib from parthenolide. These results support the development of SymProDs with α-methylene-γ-butyrolactone moiety containing NFκB inhibitors and known drugs that have secondary amine functionality as a means to target two pathways simultaneously. A similar idea was recently reported by Neumann et al., where in $_{INV}$DA led to the symbiotic formation of two active prodrugs.(Neumann, Gambardella, Lilienkampf, & Bradley, 2018)

Conclusion

In conclusion, we synthesized two amine-based prodrugs of analog **19**, which was previously reported as an NFκB pathway inhibitor. The prodrugs were more stable to biological nucleophiles, and the associated slow release was characterized by ^{19}F NMR studies. Using an alkyne-tagged prodrug (**4**), we show for the first-time engagement of NFκB pathway proteins by an analog with α-methylene-γ-butyrolactone moiety in cells. The prodrugs exhibited anticancer effects in growth inhibition assays. Using CDK inhibitors that contain solvent exposed secondary amines and NFκB inhibitors **19** and parthenolide, we synthesized 4 SymProDs. Screening these SymProDs in cell lines revealed that **19** derived SymProDs were more potent than parthenolide derived SymProDs both in cell free and cell-based assays. SymProDs are a viable path forward for advancing reactive compounds with α-methylene-γ-butyrolactone moiety as NFκB inhibitors. Additional mechanistic and *in vivo* efficacy studies with SymProDs are currently underway and will be reported in due course.

Acknowledgements

This work was supported in part by NIH grants CA182820, CA197999 and CA036727. SKo and JIC were supported by UNMC fellowship. We would like to thank the Natarajan lab members for helpful discussions.

Data Availability Statement

The data that support the findings of this study are available from the corresponding author upon request.

References:

Albert, A. (1958). Chemical aspects of selective toxicity. *Nature, 182*(4633), 421-422. Retrieved from https://www.ncbi.nlm.nih.gov/pubmed/13577867

Babak, M. V. V., Zhi, Y., Czarny, B., Toh, T. B., Ooi, L., Chow, E. K., . . . Pastorin, G. (2019). Dual-targeting Dual-action Platinum(IV) Platform for Enhanced Anticancer Activity and Reduced Nephrotoxicity. *Angew Chem Int Ed Engl*. doi:10.1002/anie.201903112

Balendiran, G. K., Dabur, R., & Fraser, D. (2004). The role of glutathione in cancer. *Cell Biochem Funct, 22*(6), 343-352. doi:10.1002/cbf.1149

Baltzer, B., Binderup, E., von Daehne, W., Godtfredsen, W. O., Hansen, K., Nielsen, B., . . . Vangedal, S. (1980). Mutual pro-drugs of beta-lactam antibiotics and beta-lactamase inhibitors. *J Antibiot (Tokyo), 33*(10), 1183-1192. Retrieved from https://www.ncbi.nlm.nih.gov/pubmed/6969724

Bork, P. M., Schmitz, M. L., Kuhnt, M., Escher, C., & Heinrich, M. (1997). Sesquiterpene lactone containing Mexican Indian medicinal plants and pure sesquiterpene lactones as potent inhibitors of transcription factor NF-kappaB. *FEBS Lett, 402*(1), 85-90. Retrieved from https://www.ncbi.nlm.nih.gov/pubmed/9013864

Cranmer, L. D. (2019). Spotlight on aldoxorubicin (INNO-206) and its potential in the treatment of soft tissue sarcomas: evidence to date. *Onco Targets Ther, 12*, 2047-2062. doi:10.2147/OTT.S145539

Curry, E. A., 3rd, Murry, D. J., Yoder, C., Fife, K., Armstrong, V., Nakshatri, H., . . . Sweeney, C. J. (2004). Phase I dose escalation trial of feverfew with standardized doses of parthenolide in patients with cancer. *Invest New Drugs, 22*(3), 299-305. doi:10.1023/B:DRUG.0000026256.38560.be

Dall'Acqua, A., Sonego, M., Pellizzari, I., Pellarin, I., Canzonieri, V., D'Andrea, S., . . . Baldassarre, G. (2017). CDK6 protects epithelial ovarian cancer from platinum-induced death via FOXO3 regulation. *EMBO Mol Med, 9*(10), 1415-1433. doi:10.15252/emmm.201607012

Gao, Y., Shen, J., Choy, E., Mankin, H., Hornicek, F., & Duan, Z. (2017). Inhibition of CDK4 sensitizes multidrug resistant ovarian cancer cells to paclitaxel by increasing apoptosiss. *Cell Oncol (Dordr), 40*(3), 209-218. doi:10.1007/s13402-017-0316-x

Guthrie, D., & Gibson, A. L. (1977). Doxorubicin cardiotoxicity: possible role of digoxin in its prevention. *Br Med J, 2*(6100), 1447-1449. Retrieved from https://www.ncbi.nlm.nih.gov/pubmed/589261

Guzman, M. L., Rossi, R. M., Neelakantan, S., Li, X., Corbett, C. A., Hassane, D. C., . . . Jordan, C. T. (2007). An orally bioavailable parthenolide analog selectively eradicates acute myelogenous leukemia stem and progenitor cells. *Blood, 110*(13), 4427-4435. Retrieved from http://www.ncbi.nlm.nih.gov/entrez/query.fcgi?cmd=Retrieve&db=PubMed&dopt=Citation&list_uids=17804695

Hall, M. D., Mellor, H. R., Callaghan, R., & Hambley, T. W. (2007). Basis for design and development of platinum(IV) anticancer complexes. *J Med Chem, 50*(15), 3403-3411. doi:10.1021/jm070280u

Harper, B. W. J., Petruzzella, E., Sirota, R., Faccioli, F. F., Aldrich-Wright, J. R., Gandin, V., & Gibson, D. (2017). Synthesis, characterization and in vitro and in vivo anticancer activity of Pt(iv) derivatives of [Pt(1S,2S-DACH)(5,6-dimethyl-1,10-phenanthroline)]. *Dalton Trans, 46*(21), 7005-7019. doi:10.1039/c7dt01054k

Hexum, J. K., Becker, C. M., Kempema, A. M., Ohlfest, J. R., Largaespada, D. A., & Harki, D. A. (2015). Parthenolide prodrug LC-1 slows growth of intracranial glioma. *Bioorg Med Chem Lett, 25*(12), 2493-2495. doi:10.1016/j.bmcl.2015.04.058

Holcomb, B. K., Yip-Schneider, M. T., Waters, J. A., Beane, J. D., Crooks, P. A., & Schmidt, C. M. (2012). Dimethylamino parthenolide enhances the inhibitory effects of gemcitabine in human pancreatic cancer cells. *J Gastrointest Surg, 16*(7), 1333-1340. doi:10.1007/s11605-012-1913-7

House, C. D., Jordan, E., Hernandez, L., Ozaki, M., James, J. M., Kim, M., . . . Annunziata, C. M. (2017). NFkappaB Promotes Ovarian Tumorigenesis via Classical Pathways That Support Proliferative Cancer Cells and Alternative Pathways That Support ALDH(+) Cancer Stem-like Cells. *Cancer Res, 77*(24), 6927-6940. doi:10.1158/0008-5472.CAN-17-0366

Kratz, F., Warnecke, A., Scheuermann, K., Stockmar, C., Schwab, J., Lazar, P., . . . Unger, C. (2002). Probing the cysteine-34 position of endogenous serum albumin with thiol-binding doxorubicin derivatives. Improved efficacy of an acid-sensitive doxorubicin derivative with specific albumin-binding properties compared to that of the parent compound. *J Med Chem, 45*(25), 5523-5533. Retrieved from https://www.ncbi.nlm.nih.gov/pubmed/12459020

Lanning, B. R., Whitby, L. R., Dix, M. M., Douhan, J., Gilbert, A. M., Hett, E. C., . . . Cravatt, B. F. (2014). A road map to evaluate the proteome-wide selectivity of covalent kinase inhibitors. *Nat Chem Biol, 10*(9), 760-767. doi:10.1038/nchembio.1582

Lee, D. F., Kuo, H. P., Chen, C. T., Hsu, J. M., Chou, C. K., Wei, Y., . . . Hung, M. C. (2007). IKK beta suppression of TSC1 links inflammation and tumor angiogenesis via the mTOR pathway. *Cell, 130*(3), 440-455. Retrieved from http://www.ncbi.nlm.nih.gov/entrez/query.fcgi?cmd=Retrieve&db=PubMed&dopt=Citation&list_uids=17693255

Leizer, A. L., Alvero, A. B., Fu, H. H., Holmberg, J. C., Cheng, Y. C., Silasi, D. A., . . . Mor, G. (2011). Regulation of inflammation by the NF-kappaB pathway in ovarian cancer stem cells. *Am J Reprod Immunol, 65*(4), 438-447. doi:10.1111/j.1600-0897.2010.00914.x

Nasim, S., & Crooks, P. A. (2008). Antileukemic activity of aminoparthenolide analogs. *Bioorg Med Chem Lett, 18*(14), 3870-3873. doi:10.1016/j.bmcl.2008.06.050

Neelakantan, S., Nasim, S., Guzman, M. L., Jordan, C. T., & Crooks, P. A. (2009). Aminoparthenolides as novel anti-leukemic agents: Discovery of the NF-kappaB inhibitor, DMAPT (LC-1). *Bioorg Med Chem Lett, 19*(15), 4346-4349. doi:10.1016/j.bmcl.2009.05.092

Neumann, K., Gambardella, A., Lilienkampf, A., & Bradley, M. (2018). Tetrazine-mediated bioorthogonal prodrug-prodrug activation. *Chem Sci, 9*(36), 7198-7203. doi:10.1039/c8sc02610f

Pan, Z., Scheerens, H., Li, S. J., Schultz, B. E., Sprengeler, P. A., Burrill, L. C., . . . Palmer, J. T. (2007). Discovery of selective irreversible inhibitors for Bruton's tyrosine kinase. *ChemMedChem, 2*(1), 58-61. doi:10.1002/cmdc.200600221

Pei, S., Minhajuddin, M., D'Alessandro, A., Nemkov, T., Stevens, B. M., Adane, B., . . . Jordan, C. T. (2016). Rational design of a parthenolide-based drug regimen that selectively eradicates acute myelogenous leukemia stem cells. *J Biol Chem, 291*(48), 25280. doi:10.1074/jbc.A116.750653

Perets, R., & Drapkin, R. (2016). It's Totally Tubular....Riding The New Wave of Ovarian Cancer Research. *Cancer Res, 76*(1), 10-17. doi:10.1158/0008-5472.CAN-15-1382

Petruzzella, E., Braude, J. P., Aldrich-Wright, J. R., Gandin, V., & Gibson, D. (2017). A Quadruple-Action Platinum(IV) Prodrug with Anticancer Activity Against KRAS Mutated Cancer Cell Lines. *Angew Chem Int Ed Engl, 56*(38), 11539-11544. doi:10.1002/anie.201706739

Petruzzella, E., Sirota, R., Solazzo, I., Gandin, V., & Gibson, D. (2018). Triple action Pt(iv) derivatives of cisplatin: a new class of potent anticancer agents that overcome resistance. *Chem Sci, 9*(18), 4299-4307. doi:10.1039/c8sc00428e

Rana, S., Bendjennat, M., Kour, S., King, H. M., Kizhake, S., Zahid, M., & Natarajan, A. (2019). Selective degradation of CDK6 by a palbociclib based PROTAC. *Bioorg Med Chem Lett*. doi:10.1016/j.bmcl.2019.03.035

Rana, S., Blowers, E. C., Tebbe, C., Contreras, J. I., Radhakrishnan, P., Kizhake, S., . . . Natarajan, A. (2016). Isatin Derived Spirocyclic Analogues with alpha-Methylene-gamma-butyrolactone as Anticancer Agents: A Structure-Activity Relationship Study. *J Med Chem, 59*(10), 5121-5127. doi:10.1021/acs.jmedchem.6b00400

Rana, S., & Natarajan, A. (2013). Face selective reduction of the exocyclic double bond in isatin derived spirocyclic lactones. *Org Biomol Chem, 11*(2), 244-247. doi:10.1039/c2ob27008k

Rautio, J., Meanwell, N. A., Di, L., & Hageman, M. J. (2018). The expanding role of prodrugs in contemporary drug design and development. *Nat Rev Drug Discov, 17*(8), 559-587. doi:10.1038/nrd.2018.46

Ren, Y., Yu, J., & Kinghorn, A. D. (2016). Development of Anticancer Agents from Plant-Derived Sesquiterpene Lactones. *Curr Med Chem, 23*(23), 2397-2420. Retrieved from https://www.ncbi.nlm.nih.gov/pubmed/27160533

Sagher, E., Hernandez, L., Heywood, C., Pauly, G. T., Young, M. R., Schneider, J., . . . Annunziata, C. M. (2014). The small molecule NSC676914A is cytotoxic and differentially affects NFkappaB signaling in ovarian cancer cells and HEK293 cells. *Cancer Cell Int, 14*, 75. doi:10.1186/s12935-014-0075-y

Shanmugam, R., Kusumanchi, P., Appaiah, H., Cheng, L., Crooks, P., Neelakantan, S., . . . Sweeney, C. J. (2011). A water soluble parthenolide analog suppresses in vivo tumor growth of two tobacco-associated cancers, lung and bladder cancer, by targeting NF-kappaB and generating reactive oxygen species. *Int J Cancer, 128*(10), 2481-2494. doi:10.1002/ijc.25587

Shanmugam, R., Kusumanchi, P., Cheng, L., Crooks, P., Neelakantan, S., Matthews, W., . . . Sweeney, C. J. (2010). A water-soluble parthenolide analogue suppresses in vivo prostate cancer growth by targeting NFkappaB and generating reactive oxygen species. *Prostate, 70*(10), 1074-1086. doi:10.1002/pros.21141

Solca, F., Dahl, G., Zoephel, A., Bader, G., Sanderson, M., Klein, C., . . . Adolf, G. R. (2012). Target binding properties and cellular activity of afatinib (BIBW 2992), an irreversible ErbB family blocker. *J Pharmacol Exp Ther, 343*(2), 342-350. doi:10.1124/jpet.112.197756

White, K. L., Rider, D. N., Kalli, K. R., Knutson, K. L., Jarvik, G. P., & Goode, E. L. (2011). Genomics of the NF-kappaB signaling pathway: hypothesized role in ovarian cancer. *Cancer Causes Control, 22*(5), 785-801. doi:10.1007/s10552-011-9745-4

Woods, J. R., Mo, H., Bieberich, A. A., Alavanja, T., & Colby, D. A. (2011). Fluorinated amino-derivatives of the sesquiterpene lactone, parthenolide, as (19)f NMR probes in deuterium-free environments. *J Med Chem, 54*(22), 7934-7941. doi:10.1021/jm201114t

Zaro, B. W., Whitby, L. R., Lum, K. M., & Cravatt, B. F. (2016). Metabolically Labile Fumarate Esters Impart Kinetic Selectivity to Irreversible Inhibitors. *J Am Chem Soc, 138*(49), 15841-15844. doi:10.1021/jacs.6b10589

Figure Legends

Figure 1: Stability and kinetics of release studies with a prodrug (19-AP1) of the NFκB inhibitor (19). (A) Structures of the NFκB inhibitor **19** and its amino prodrug **19-AP1**, and **19AP2**. (B) Cysteine reactivity assay used to compare the relative reactivity of the **19-AP1** and **19** towards cysteine. (C) ^{19}F NMR study to monitor the kinetics of the conversion of **19-AP1** to **19** as a function of free 4-trifluoromethylpiperidine.

Figure 2: Synthesis of an alkyne-tagged 19-AP1 (4) and cellular target engagement studies. (A) Synthetic scheme that was used for the generation of the alkyne-tagged 19-AP1 analog (**4**). (B) Cancer cells (A2780) were incubated with 10μM of analog **4** for 24h. In the cells analog **4** will be converted to analog **3** with an active methylene group which will react with surface exposed cysteine residues on proteins. The above lysate was subjected to click reagents (TCEP, TBTA and $CuSO_4$) and azido-biotin. Biotin-tagged-**3**-bound proteins were subjected to mono-avidin column. Biotin-tagged proteins were captured, the column was washed to removed untagged proteins and the biotin-tagged-**3**-bound proteins were eluted with regeneration buffer (6M urea/PBS). The eluted lysates were subjected to Western blot analyses and probed for proteins (IKKβ, RELA, IκBα and IKKγ) in the IKK complex.

Figure 3: Growth inhibition assays with NFκB inhibitor and its prodrugs. (A-C) Dose response studies with analog 19, 19-AP1 and 19-AP2 in ovarian cancer cell line A2780, immortalized fallopian tube epithelial cells FT282E1 and ovarian cancer cell line OVSAHO. (D) Table shows the IC50 values derived from curve fitting the growth inhibition data and the glutathione levels in A2780, FT282E1 and OVSAHO cell lines. (E) Plausible mechanism for the conversion of the prodrug to the active drug.

Figure 4: Symbiotic Prodrugs (SymProDs) of NFκB and CDK inhibitors. (A) Structure of the symbiotic prodrugs generated from CKD4/6 inhibitor palbociclib, CDK2/5/9 inhibitor AT7519 and

NFκB inhibitors **19** and parthenolide. The CDK inhibitors are shown in blue. SymProd **5** (palbociclib + **19**), SymProd **6** (palbociclib + parthenolide), SymProd **7** (AT7519 + **19**) and SymProd **8** (AT7519 + parthenolide). (B) Evaluation of palbociclib, SymProDs **5** and **6** in CDK4 and CDK6 *in vitro* kinase assays

Figure 5: SymProDs screened for growth inhibitory activity. Summary of growth inhibition assays in FTE282E1, OVSAHO, HPNE, MiaPaCa2 and S2013 cell lines with palbociclib, AT7519, **19**, parthenolide, (1:1) combinations and the corresponding SymProDs (**5**-**8**) (n= 3, bar graph is Mean $\pm$ SD)

Figure 6: Growth inhibition assays in a panel of Ovarian cell lines. Growth inhibition assays in a panel of 11 cell lines (9 ovarian cancer cell lines and 2 immortalized fallopian tube epithelial cell lines) with SymProDs **5** and **6** and their corresponding 1:1 mixture. (n = 3)

Figure 1

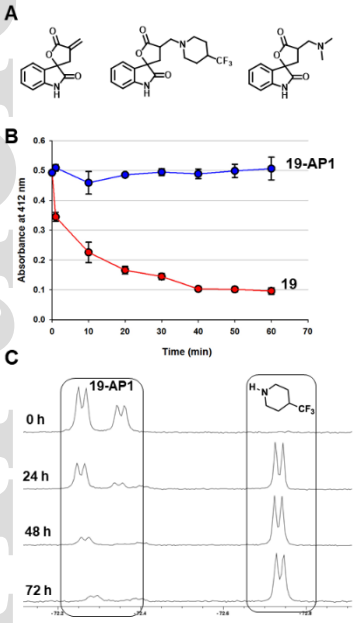

Figure 2

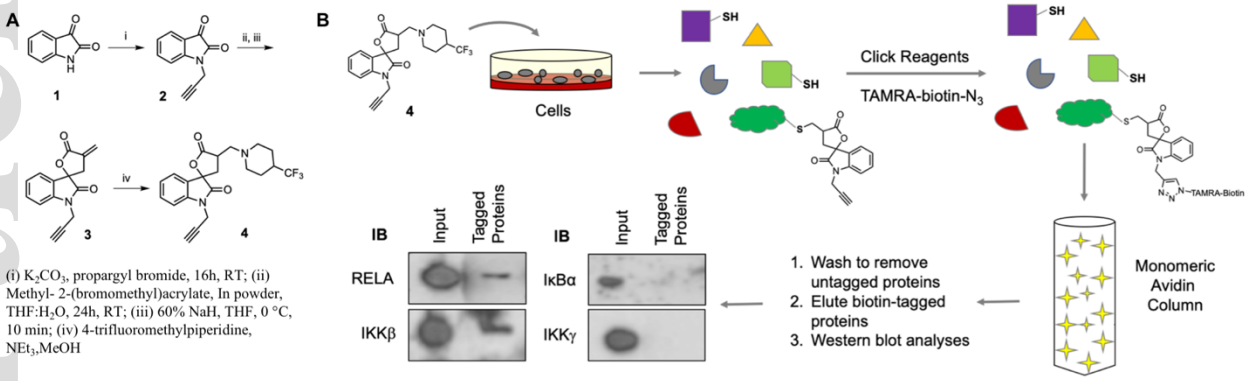

Figure 3

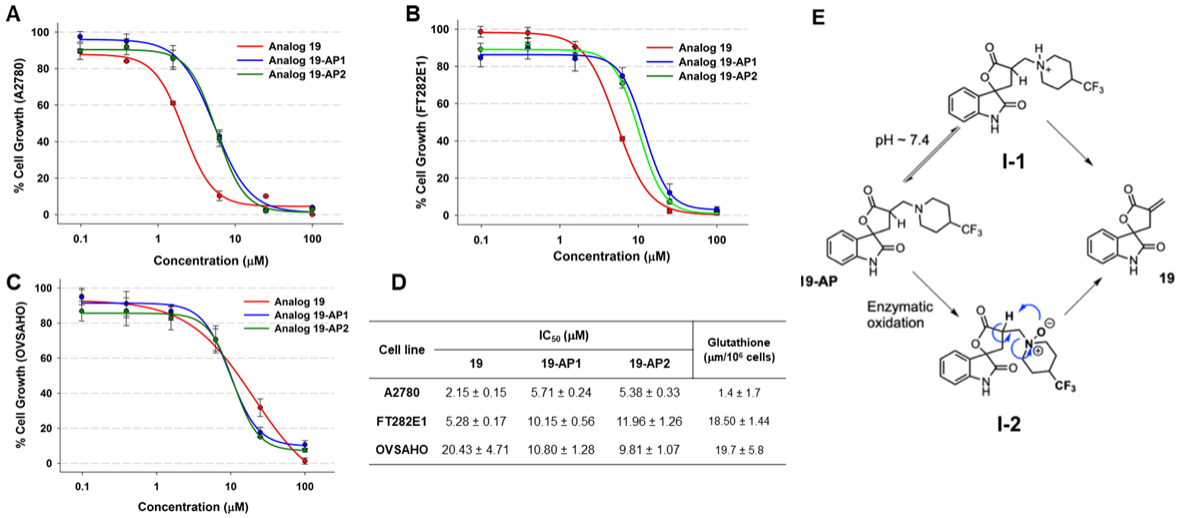

Cell line	IC_{50} (μM)			Glutathione (μm/10^6 cells)
	19	19-AP1	19-AP2	
A2780	2.15 ± 0.15	5.71 ± 0.24	5.38 ± 0.33	1.4 ± 1.7
FT282E1	5.28 ± 0.17	10.15 ± 0.56	11.96 ± 1.26	18.50 ± 1.44
OVSAHO	20.43 ± 4.71	10.80 ± 1.28	9.81 ± 1.07	19.7 ± 5.8

Figure 4

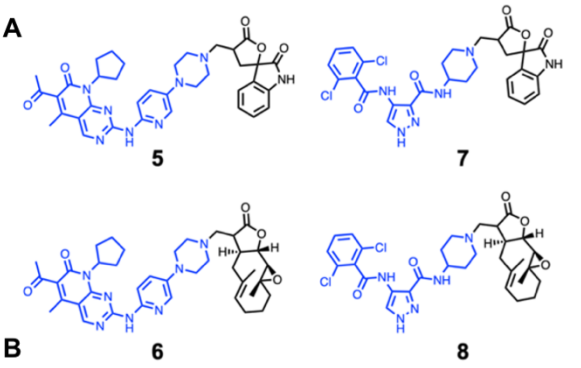

Kinase	IC_{50} (nM)		
	Palbociclib	5	6
CDK4	< 0.38	46 ± 14	85 ± 18
CDK6	< 0.38	9 ± 1	18 ± 1

Figure 5

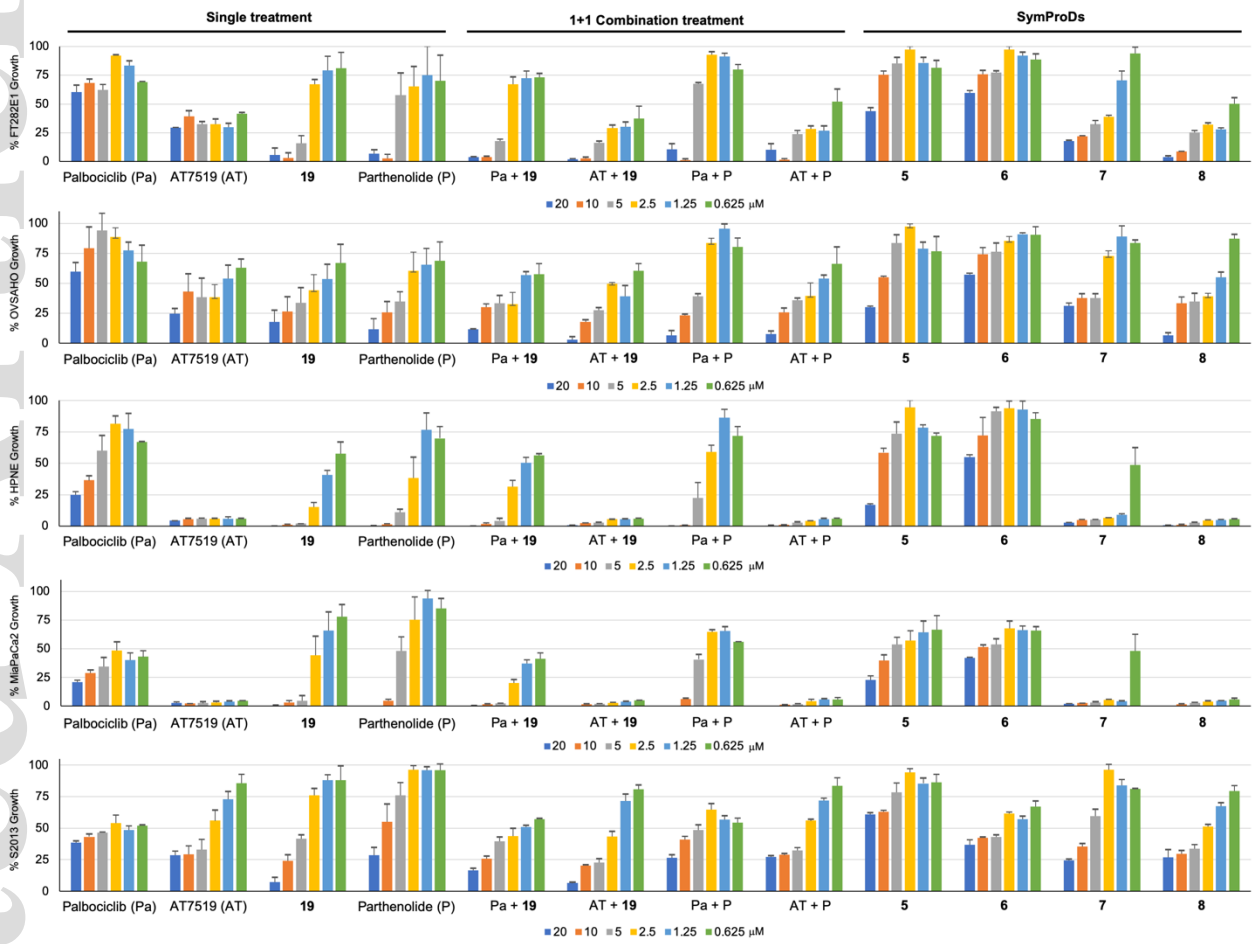

Figure 6

Cell line	IC_{50} (Mean ± SD μM)			
	Palbociclib + **19**	**5**	Palbociclib + Parthenolide	**6**
FT282E1	9.8 ± 8.3	14.6 ± 1.2	9.1 ± 0.6	> 40
FT282C11	17.6 ± 0.9	21.8 ± 1.5	9.8 ± 0.4	25.6 ± 4.8
CaOV3	5.3 ± 0.5	5.5 ± 0.5	5.6 ± 0.2	25.0 ± 3.2
OVCAR5	5.1 ± 0.5	9.3 ± 0.9	6.2 ± 0.2	32.6 ± 4.4
OVCAR8	7.6 ± 0.7	9.1 ± 0.9	6.4 ± 0.5	38.4 ± 4.5
A2780	9.6 ± 1.4	6.6 ± 1.3	6.1 ± 0.7	31.0 ± 7.0
Kuramochi	28.0 ± 3.0	> 40	9.8 ± 1.2	> 40
OVCAR4	12.7 ± 0.7	17.9 ± 1.4	11.8 ± 2.4	> 40
OVSAHO	12.4 ± 4.0	11.4 ± 0.9	3.2 ± 0.2	31.1 ± 2.3
SKOV3	14.2 ± 1.2	15.4 ± 1.5	4.5 ± 0.8	> 40
SNU119	20.5 ± 2.1	8.8 ± 1.6	2.9 ± 0.4	34.9 ± 6.3